Effects of exchange frustrations in $NdMn_2$

1992 J. Phys.: Condens. Matter 4 4675

(http://iopscience.iop.org/0953-8984/4/19/010)

J. Phys.: Condens. Matter 4 (1992) 4675–4686. Printed in the UK

Effects of exchange frustrations in $NdMn_2$

B Ouladdiaf†, R Ballou‡, J Deportes‡, R Lemaire§ and F Sayetat||

† Institut Laue–Langevin, 156X, 38042 Grenoble Cédex, France
‡ Laboratoire de Magnetisme L Néel, CNRS, 166X, 38042 Grenoble Cédex, France
§ Centre Universitaire, Evry-Val D'Essone, Boulevard Des Coquibus, 91025 Evry, France
|| Laboratoire de Crystallographie, CNRS, 166X, 38042 Grenoble Cédex, France

Received 28 November 1991

Abstract. Magnetic ordering in $NdMn_2$ has been studied by magnetization measurements and powder x-ray and neutron diffraction experiments. Giant magnetoelastic effects giving rise to both a large magnetovolume effect and a monoclinic crystal distortion at the magnetic ordering are found. A magnetic structure with two different propagation vectors and an unusual decoupling phenomenon is deduced. All these effects are discussed and shown to lead to reduction in the high frustration of the Mn magnetism in $NdMn_2$. A reorientation process involving the Nd moments and only a quarter of the Mn moments is also found with decreasing temperature and is discussed in terms of the Mn and Nd anisotropy.

1. Introduction

The intermetallic RMn_2 Laves phase compounds (where R stands for Y, Sc, Th or a lanthanide) are currently the subject of intense experimental investigation since the behaviour of Mn in these compounds provides an attractive opportunity for studying itinerant electron antiferromagnetic instability in a highly frustrated lattice.

According to the R species, Mn may either remain non-magnetic or exhibit a large moment. It has been suggested that a Mn moment is stabilized only for a Mn–Mn spacing larger than a critical value [1]. In the case where this is achieved, the Mn–Mn magnetic interactions in the compounds become dominant and impose an antiferromagnetic arrangement of the moments [2]. The magnetism of the R ions is then superimposed without inducing fundamental modifications except for second-order effects.

The RMn_2 compounds crystallize in either the hexagonal C14 or the cubic C15 Laves phase. In both structures the Mn atoms are located at the corners of regular tetrahedra. These tetrahedra are stacked in a summit-to-summit and base-to-base sequence in the hexagonal phase and in the corner-sharing sequence in the cubic phase. In the topology of these structures all antiferromagnetic orderings are subject to strong frustration of the magnetic interactions.

Owing to the high frustration of the magnetic interactions a variety of complex magnetic structures could *a priori* be stabilized. Among these different possible structures, the actual magnetic ground state found experimentally is that which minimizes the frustration, through extra degrees of freedom of the systems such as large magnetoelastic effects. Instability of the Mn moment may also be highly relevant, leading

0953-8984/92/194675+12$04.50

to exotic inhomogeneous cancellation of the moment as shown in $DyMn_2$ [3]. In $ThMn_2$ (where Th is non-magnetic) when the antiferromagnetic order occurs below 115 K, one Mn atom out of four remains non-magnetic while the others order with a triangular configuration. This non-magnetic state of some Mn atoms together with the large anisotropic thermal expansion effects observed in this compound minimize the frustration [2, 4].

In this paper we report a study, by means of magnetization data and x-ray and neutron diffraction, of the mechanisms which yield a reduction in the frustration of the hexagonal $NdMn_2$ compound. Experiments were carried out on polycrystalline samples prepared by induction melting and subsequently annealed for 7 days at 840 °C.

2. Magnetic properties

Isotherms of the field dependence of the magnetization have been measured in fields H up to 60 kOe at different temperatures T between 2 and 300 K, some of which are reported in the inset of figure 1. In the whole temperature range of the measurements they are nearly linear except at low temperatures where a slight curvature is observed for high values of the applied field. Also reported in figure 1, is the thermal dependence of the initial magnetic susceptibility χ deduced from the measured isotherms. It shows a large discontinuity (30%) coupled with a 2 K hysteresis, characteristic of a first-order transition. With increasing temperature, magnetic ordering is found to occur at $T_N = 105$ K (upper bound of the thermal hysteresis). All these results are in good agreement with previous data [5, 6].

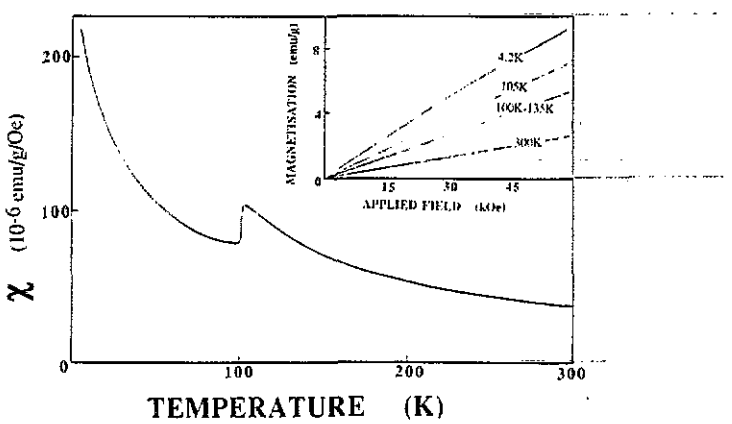

Figure 1. Thermal variation in the magnetic susceptibility of $NdMn_2$. The inset shows the field dependence of the magnetization at various temperatures.

Above the Néel temperature T_N, the initial magnetic susceptibility of the compound decreases with increasing temperature, according to the following modified Curie–Weiss law: $\chi(T) = \chi b + C_{Nd^{3+}}/(T - \Theta)$, where $C_{Nd^{3+}}$ is the Curie constant calculated for the Nd^{3+} ion (effective moment, 3.62 μ_B). χb stands for a band conduction susceptibility, taken to be temperature independent in comparison with the magnetic susceptibilities of YMn_2 and $ThMn_2$ which are weakly temperature dependent [6]. Θ could be interpreted as a paramagnetic Curie temperature associated

with all the exchange interactions involving the Nd magnetism. By fitting the experimental curve, the two unknown parameters χb and Θ were found to be respectively $\chi b = 13 \times 10^{-6}$ emu g^{-1} Oe^{-1} and $\Theta = 37$ K. χb is about two times larger than in YMn_2 (6×10^{-6} emu g^{-1} Oe^{-1}) [5] and in $ThMn_2$ (8×10^{-6} emu g^{-1} Oe^{-1}) [2], an enhancement which should be correlated with the Nd–Mn exchange interactions. Θ is a third of T_N which, owing to the frustration, gives only a lower limit for the Mn–Mn exchange interactions.

In short, as for YMn_2, the discontinuity of the initial magnetic susceptibility of $NdMn_2$ should be correlated with a first-order antiferromagnetic transition governed essentially by the Mn–Mn magnetic interactions.

3. Crystallographic properties

$NdMn_2$ crystallizes in the C14 hexagonal Laves phase ($MgZn_2$ type). The space group is $P6_3/mmc$ (D^4_{6h}). Mn occupies two different crystallographic sites: 6h (local symmetry, mm) and 2a (local symmetry, $\bar{3}m$). Nd is located in the 4f site (local symmetry, $3m$). The lattice parameters at 300 K were determined as $a_h = 5.554$ Å and $c_h = 9.051$ Å. A schematic view of the structure is given in figure 2. Mn atoms are located at the corners of regular tetrahedra stacked in a base-to-base and summit-to-summit sequence to form chains along the sixfold axis. Adjacent chains join to form layers perpendicular to the sixfold axis defining a 'Kagomé network' of the Mn atoms of the 6h site.

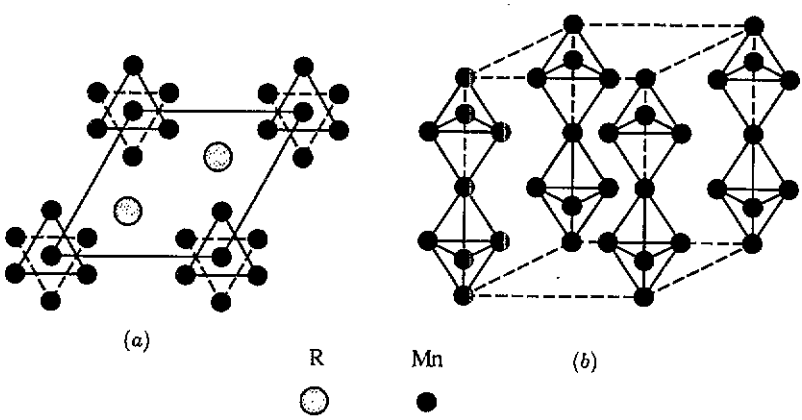

Figure 2. Crystallographic structure of the hexagonal Laves phases C14: (*a*) projection in the (001) plane; (*b*) stacking of Mn tetrahedra.

Powder x-ray diffraction measurements have been carried out between 2.2 and 300 K, using the Cr $K\alpha_1$ radiation ($\lambda = 2.289\,62$ Å), on a Seemann–Bohlin diffractometer. Crystal lattice parameters were deduced from the thermal evolution of three diffraction peaks (220), (004) and (107), with fairly good relative precision.

In the 105–300 K temperature range, the crystal structure is hexagonal and the lattice parameters follow the usual Debye law. The thermal expansion coefficients were found to be $\alpha_a = 3 \times 10^{-5}$ K^{-1}, $\alpha_c = 4 \times 10^{-5}$ K^{-1} and $\beta_{volume} = 10^{-4}$ K^{-1}, at 250 K (figure 3), which are twice the values of similar coefficients for other intermetallic compounds [7, 8].

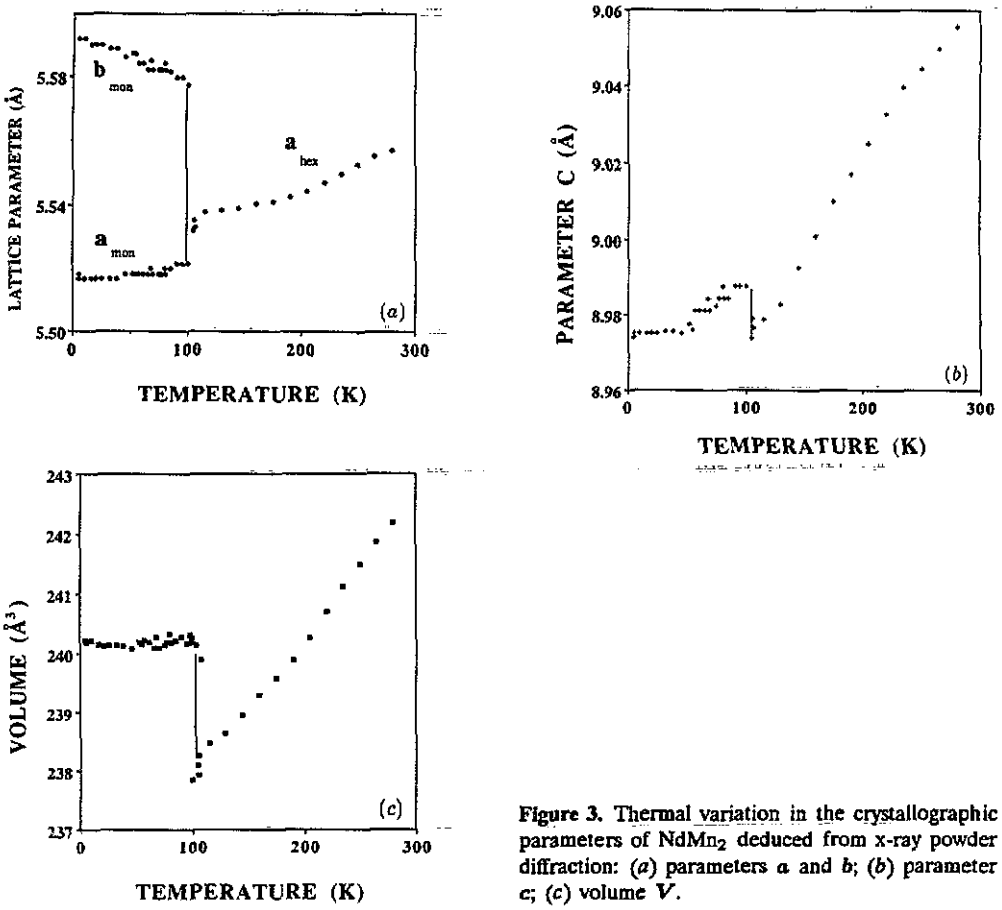

Figure 3. Thermal variation in the crystallographic parameters of $NdMn_2$ deduced from x-ray powder diffraction: (*a*) parameters *a* and *b*; (*b*) parameter *c*; (*c*) volume *V*.

At lower temperatures, drastic changes appear in the pattern: all the $(hk0)$ reflections are split while the $(00l)$ reflections remain unchanged. In fact, the (220) hexagonal reflection gives rise to three peaks of about equal intensity which could be indexed as (220), $(\bar{2}40)$ and $(\bar{4}20)$ in a monoclinic description of the crystal structure. A large monoclinic distortion is thus shown when the magnetic ordering sets in. It occurs only in the basal plane perpendicular to the sixfold axis of the paramagnetic phase.

At liquid-helium temperature, the lattice parameters of the monoclinic cell were determined as $a_m = 5.5210(5)$ Å, $b_m = 5.5770(5)$ Å, $c = 8.9870(5)$ Å and $\gamma = 119.80(1)°$. Figure 4 shows the thermal dependence of ϵ defined by $\epsilon = 120° - \gamma$. It may be taken as an order parameter. The three possible monoclinic groups, subgroups of $P6_3/mmc$, are $P2_1/m$, $P2_1$ or Pm. In the $P2_1/m$ group, the Mn 6h site of the hexagonal structure is split into three inequivalent 2e sites while the Mn 2a and Nd 4f sites keep their multiplicity (table 1).

Thus, with decreasing temperature, $NdMn_2$ undergoes a first-order phase transition below 105 K (within 2 K) with obvious discontinuities in all the cell parameters and a relative variation in the *c* parameter of +0.9%, inducing a volume increase of 0.9%. Our results are in good agreement with those of Tagawa *et al* [9] but have

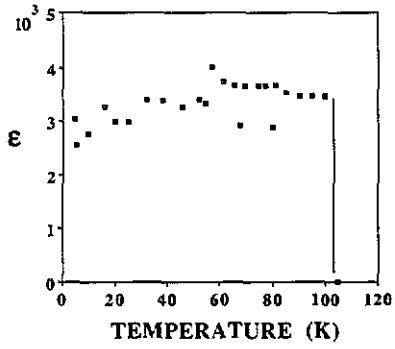

Figure 4. Thermal dependence of the order parameter $\epsilon = 120° - \gamma$.

better accuracy because of the use of diffraction peaks at large scattering angles.

4. Neutron diffraction

Neutron diffraction experiments were performed using a multidetector spectrometer with a neutron wavelength $\lambda_N = 2.503$ Å at the Grenoble Nuclear Centre. Several neutron diffraction patterns were obtained above and below $T_N = 105$ K, which were quantitatively studied by least-squares refinement on integrated intensities. Above 105 K (figure 5), the pattern contains only nuclear peaks, all consistent with the C14 Laves phase structure; the agreement between the calculated and observed diffraction peaks, using $b_{Mn} = -0.36 \times 10^{-12}$ cm and $b_{Nd} = 0.75 \times 10^{-12}$ cm as scattering lengths, yields a reliability factor R of 6% where $R = \sum(I_{obs} - I_{cal}) / \sum I_{obs}$. Below T_N, some peaks (102, 110, 103, 200, ...) are split and this splitting is consistent with monoclinic distortion. However, the $P2_1$ group is incompatible with $(00l)$ reflections when l is odd. So, $P2_1$ is discarded. Furthermore, some supplementary non-nuclear peaks are observed. Because of a good knowledge of the monoclinic distortion, they can be indexed as $K_1 = [\frac{1}{2}00]$ propagation vector (group I) or as $K_2 = [0\frac{1}{2}0]$ propagation vector (group II). The intensities of the peaks belonging to group II increase with decreasing temperature (figures 5 and 6) below about 50 K. However, those of group I are almost temperature independent. Thus, the $(\frac{1}{2}h\,k\,l)$ reflections are characteristic mainly of the Mn–Mn interactions while the $(h\,\frac{1}{2}k\,l)$ reflections are characteristic of the Mn–Nd interactions. So, as already explained, the Mn_I–Mn_I interactions govern the first-order transition at 105 K, while the Mn_I–Nd interactions and some Nd–Mn_{II} interactions may induce a modification of the magnetic structure below 50 K. The existence of two such groups, i.e. two magnetic propagation vectors, leads to uncoupled magnetic sublattices and the magnetic cell $(2a_m, 2b_m, c)$ is then four times larger than the crystallographic cell.

The refinement of the neutron diffraction data at low temperatures suggests that, in the magnetically ordered state of $NdMn_2$, the Nd atoms have two types of magnetic environment. The molecular field acting on one of these Nd sites (marked 1 in figure 7) is $4n'M_{Mn}$ whereas it is $2n'M_{Mn}$ on the other (marked 2 in figure 7), where n' is the Mn–Nd molecular field coefficient and M_{Mn} is the Mn moment. As a consequence the corresponding space group is Pm (a subgroup of $P2_1/m$) rather than $P2_1/m$. Using the Pm space group, the result of the refinement of the magnetic intensities is significantly improved: the reliability factors are 5% at 100 K

Table 1. Crystallographic parameters in the hexagonal and monoclinic phases of $NdMn_2$ (above and below T_N).

Hexagonal structure $P6_3/mm$ origin at centre $(\bar{3}m1)$				Monoclinic structure $P2_1/m$ origin at $\bar{1}$				Monoclinic structure Pm origin at m			
	Position				Position				Position		
Atom	Site	Coordinates	Site symmetry	Atom	Site	Coordinates	Site symmetry	Atom	Site	Coordinates	Site symmetry
Mn	2a	0,0,0 $0,0,\frac{1}{2}$	$\bar{3}m$	Mn	2a	0,0,0 $0,0,\frac{1}{2}$	$\bar{1}$	Mn	2c	x,y,z $x,y,-z$ $(x=0,y=0,z=\frac{1}{4})$	1
Mn			mm	Mn	$2e_1$	$x,y,\frac{1}{4}$ $x,y,\frac{3}{4}$ $(x=-\frac{1}{6},y=\frac{1}{6})$	m	Mn	1a	$x,y,0$ $(x=-\frac{1}{6},y=\frac{1}{6})$	m
									1b	$x,y,\frac{1}{2}$ $(x=-\frac{1}{6},y=-\frac{1}{6})$	
	6h	$x,-x,\frac{1}{4}$ $-x,x,\frac{3}{4}$ $2-x,-x,\frac{1}{4}$ $2x,x,\frac{3}{4}$ $x,2x,\frac{1}{4}$ $-x,2-x,\frac{3}{4}$ $(x=-\frac{1}{6})$			$2e_2$	$x,y,\frac{1}{4}$ $-x,-y,\frac{3}{4}$ $(x=-\frac{2}{6},y=\frac{1}{6})$			1a	$x,y,0$ $(x=\frac{2}{6},y=\frac{1}{6})$	
									1b	$x,y,\frac{1}{2}$ $(x=-\frac{2}{6},y=-\frac{1}{6})$	
					$2e_3$	$x,y,\frac{1}{4}$ $-x,-y,\frac{3}{4}$ $(x=-\frac{1}{6},y=-\frac{2}{6})$			1a	$x,y,0$ $(x=-\frac{1}{6},y=-\frac{2}{6})$	
									1b	$x,y,\frac{1}{2}$ $(x=\frac{1}{6},y=-\frac{2}{6})$	

Table 1. Continued.

Nd	4f	$\frac{1}{3},\frac{2}{3},z$ $\frac{2}{3},\frac{1}{3},-z$ $\frac{1}{3},\frac{2}{3},\frac{1}{2}-z$	$3m$	Nd	4f	x,y,z $-x,-y,-z$ $x,y,\frac{1}{2}-z$	1	Nd	$2c_1$	x,y,z $x,y,-z$ $(x=\frac{2}{3},y=\frac{1}{3},z=\frac{5}{16})$	1
		$\frac{2}{3},\frac{1}{3},\frac{1}{2}+z$ $(z=\frac{1}{16})$				$-x,-y,\frac{1}{2}+z$ $(x=\frac{1}{3},y=\frac{2}{3},z=\frac{1}{6})$			$2c_2$	x,y,z $x,y,-z$ $(x=\frac{1}{3},y=\frac{2}{3},z=\frac{3}{16})$	1

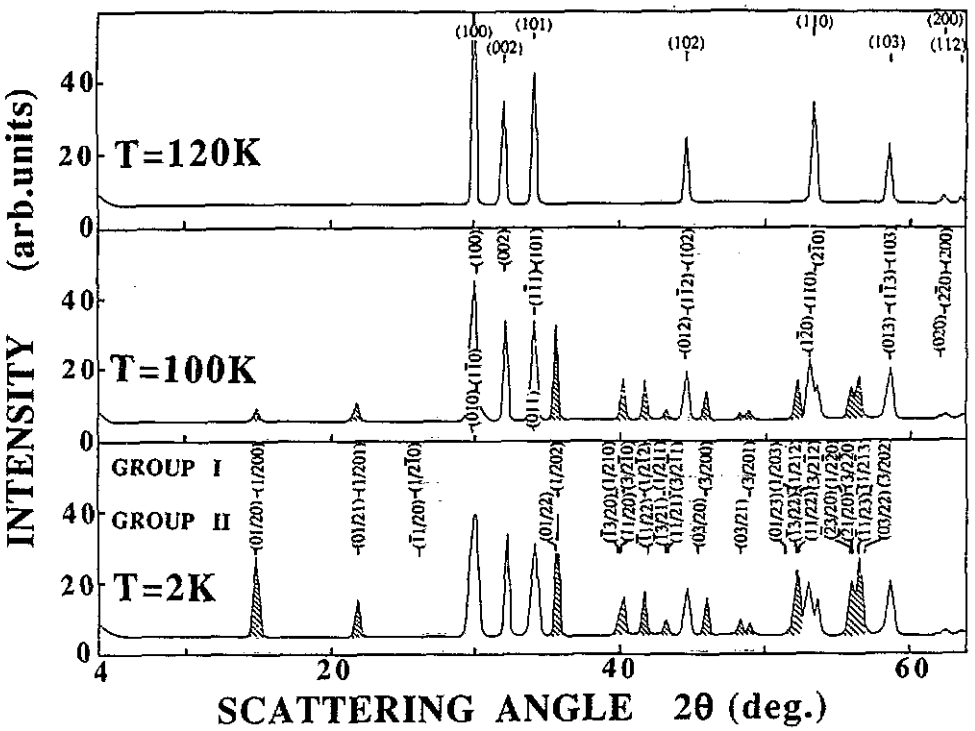

Figure 5. Powder neutron diffraction data for $NdMn_2$ measured at 120, 100 and 2 K with $\lambda = 2.483$ Å. The magnetic peaks are indexed by $K_1 = [\frac{1}{2}00]$ for group I and $K_2 = [0\frac{1}{2}0]$ for group II in the monoclinic cell.

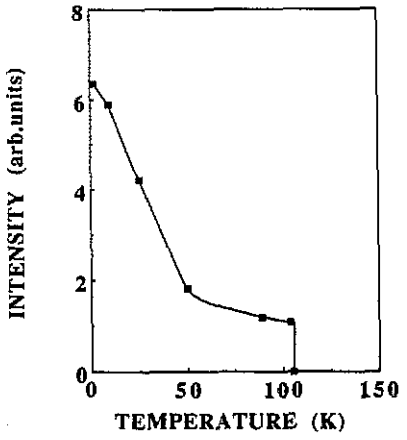

Figure 6. Thermal dependence of the intensity of the $(0\frac{1}{2}0)$ characteristic of the spin rotation of $NdMn_2$ below 50 K.

and 6% at 2 K. The resulting moments are listed in table 2. In this description, the Mn atoms which occupied the 6h site above T_N are instead located in three 1a and three 1b sites (symmetry, m), the Mn atoms which occupied the 2a sites (symmetry $\bar{3}m$) keep their multiplicity (2c; symmetry 1) while the Nd which occupied the 4f sites (symmetry, $3m$) are in two different 2c sites ($2c_1$ and $2c_2$; symmetry, 1). Figure 8 presents the magnetic environments of the two Nd sites in detail. In table 1 we have summarized the crystallographic parameters obtained after refinement. Although the

data are best represented by the Pm space group, we continue to use the notation of the $P2_1/m$ space group in the rest of the paper.

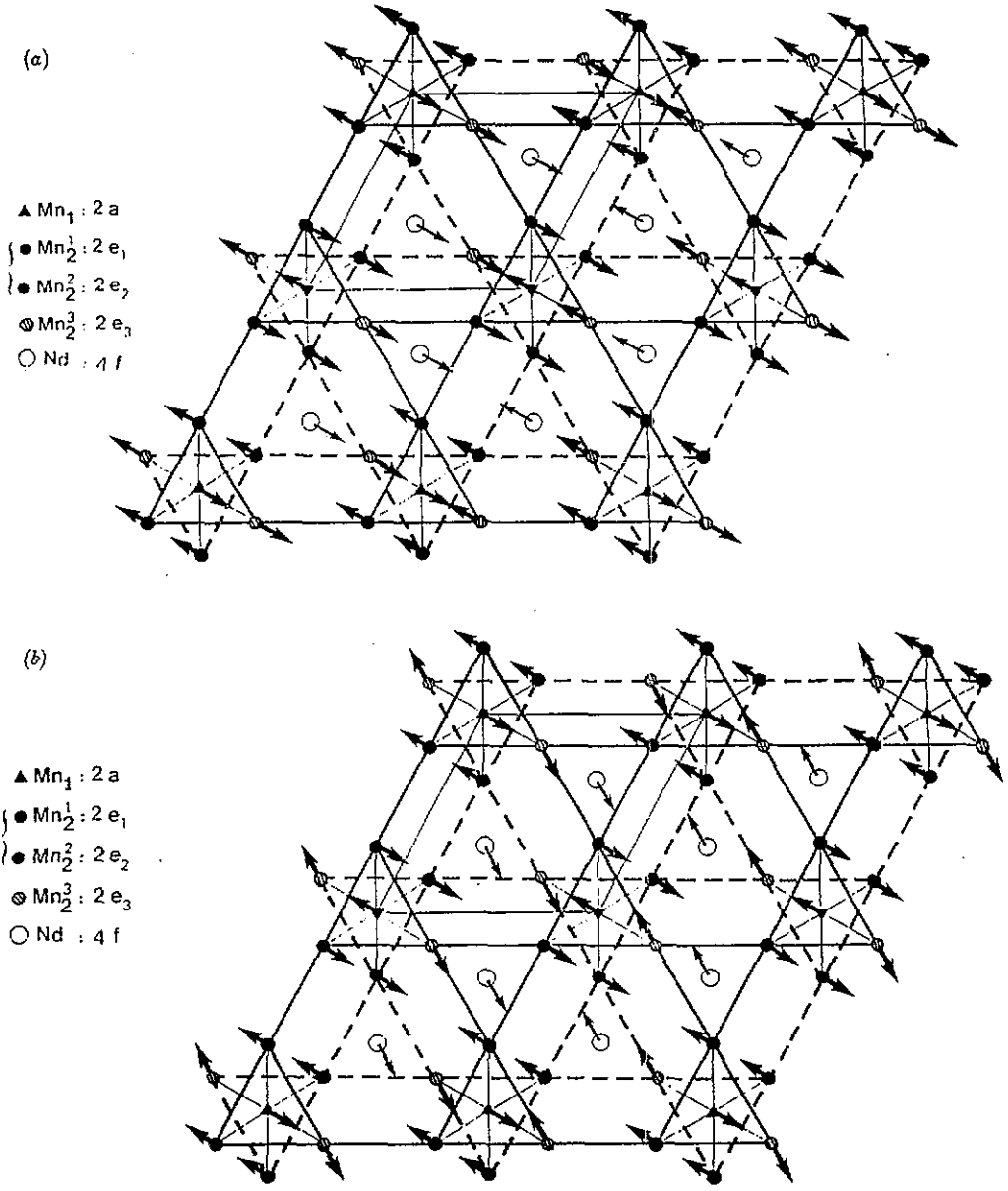

Figure 7. Projection on the basal plane of the magnetic structure of $NdMn_2$ deduced from powder neutron diffraction data: (*a*) the magnetic structure above 50 K; (*b*) the magnetic structure at 2 K (the moments of group I are parallel to the [120] axis, and those of group II are parallel to [110]).

The magnetic arrangements below 105 K and below 50 K are fairly sophisticated. Below 105 K, a collinear antiferromagnetic arrangement in the basal plane occurs. As already explained, the framework is constituted from chains of Mn tetrahedra along

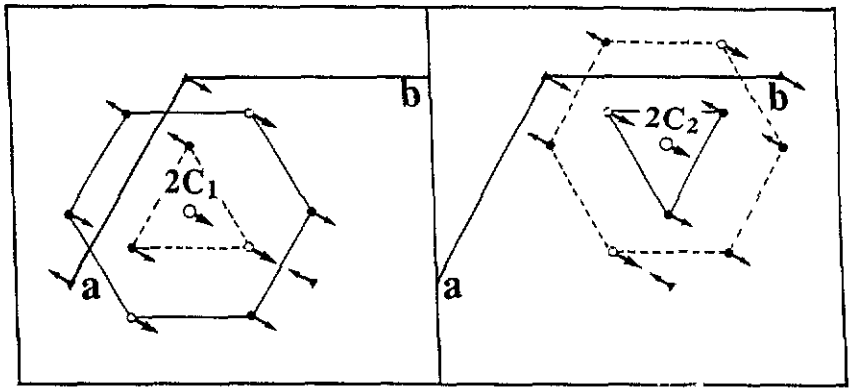

Figure 8. Magnetic environment of Nd moments of the $2c_1$ and $2c_2$ sites of $NdMn_2$ in the Pm space group.

Table 2. Magnetic moments of $NdMn_2$ in the monoclinic structure, deduced from neutron powder neutron diffraction refinement at 100 and 2 K.

T	Magnetic moment (μ_B)				
(K)	Mn (2c)	Mn(1a)	Mn(1b)	Nd($2c_1$)	Nd($2c_2$)
100	2.4	2.4	2.4	2.05	1.7
2	2.7	2.7	2.7	2.9	2.9

a and half these chains are antiferromagnetically coupled along b while all the chains are antiferromagnetically coupled along a.

Below 50 K, the thermal dependence of some peaks $(0\ \frac{1}{2}k\ 0)$ (group II) (figure 6) is explained by a progressive rotation of about 30° from the [120] axis of the Nd moments and of the Mn_{II} moments (those originating from the $2e_3$ site). In this description, the c axis is only a 2_1 axis for Nd and Mn_{II} moments while it is a $2'_1$ antiaxis for the Mn_I moments.

A schematic diagram of the coupling inside the magnetic structures at 100 K and at 2 K is shown in figure 9.

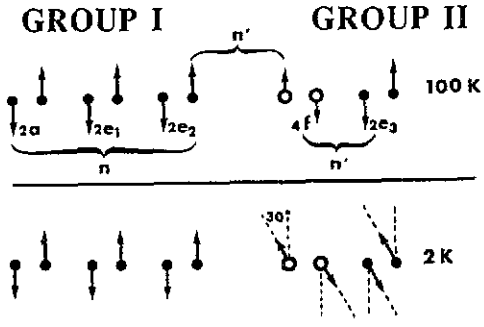

Figure 9. Schematization of the magnetic coupling of $NdMn_2$ deduced from the magnetic structure.

5. Discussion

Frustration is due to the existence, in any magnetic arrangement, of pairs of moments for which antiferromagnetic coupling is not achieved. The corresponding cost in energy $2J_{ij}\boldsymbol{S}_i \cdot \boldsymbol{S}_j$ can be lowered in several ways. This can be achieved through the dependence of the exchange integral J_{ij} upon interatomic distances. Other effects are related to the trigonometry associated with the $\boldsymbol{S}_i \cdot \boldsymbol{S}_j$ scalar product [2]. In the case of an itinerant antiferromagnet close to its instability, the spin amplitude becomes an extra degree of freedom which allows an additional reduction of exchange energy in frustrated nearest-neighbour pairs [10, 11].

The first-order transition at T_N is mainly governed by Mn–Mn interactions (group I), yielding an antiferromagnetic collinear arrangement in the basal plane along $[0\frac{1}{2}0]$. Nd moments (group II) lie in the same direction, in an antiferromagnetic configuration as paramagnetic ions in the exchange field due to Mn moments (group I). Finally, Mn moments (group II) are oriented parallel to Nd moments through the exchange field due to the rare-earth ions. Indeed the molecular field resulting from the first-nearest-neighbour Mn moments of group I cancels on the $2e_3$ site. This planar magnetic configuration is accompanied by a sudden shrinkage in the c parameter, yielding a volume reduction.

At low temperatures, the reorientation of the Nd moments, especially detectable below 50 K (figure 6), is governed by the anisotropic crystal field acting on Nd (which increases strongly with decreasing temperature) and is favoured by the weak Nd–Mn_I exchange interaction. So with decreasing temperature the Nd moments rotate progressively away from the [120] axis towards the [110]. At 4 K the rotation angle is about 30°. The Mn moments (group II) follow the Nd moments through the Nd–Mn_{II} exchange interaction (the local magnetocrystalline anisotropy is weak). On the other hand, the Mn moments (group I) do not change direction because the Nd–Mn_I interaction is rather weak and the local anisotropy acting on Mn_I is fairly strong. This configuration is compatible with the observed monoclinic distortion which increases as the moment reorientation takes place. Note that the anisotropic planar distortion (large increase along b and decrease along a) is in good agreement with the ferromagnetic coupling along b and the antiferromagnetic coupling along a, respectively.

As the temperature decreases, the Mn moments are split into two sublattices I and II, which are nearly independent. This quasi-independence of the Mn_{II} moments contributes to the reduction in the magnetic frustration. This situation is to be compared with the behaviour of some of the Mn atoms (site 2a) in $ThMn_2$ which lose their magnetic moment [2]. In $NdMn_2$, the Mn_{II} atoms keep only the magnetic moment induced by the molecular field due to Nd ions. Furthermore, as the exchange interactions strongly depend on the interatomic distances, they are obviously modified at the first-order transition owing to the anisotropic-distortion-inducing reduction in the frustration.

6. Conclusion

In summary, the magnetic structure of $NdMn_2$ shows strong frustration of the antiferromagnetic interactions between first-neighbour manganese ions. The large monoclinic distortion must be related not only to the dependence of the exchange interaction on atomic distance but also to the instability of the Mn magnetic moment. The

splitting of the Mn moments into two independent quasi-sublattices is associated with minimization of the frustrated exchange energy of the Mn_I–Nd interactions coupling the two sublattices.

Acknowledgments

The authors wish to thank Dr P J Brown for helpful discussions.

References

[1] Wada H, Nakamura H, Yoshimura K, Shiga M and Nakamura Y J 1987 *J. Magn. Magn. Mater.* **70** 134
[2] Deportes J, Lemaire R, Ouladdiaf B, Roudault E and Sayetat F 1987 *J. Magn. Magn. Mater.* **70** 191
[3] Wada H, Yoshimura K, Shiga M, Goto T and Nakamura Y 1985 *J. Phys. Soc. Japan* **54** 3543
[4] Ouladdiaf B 1986 *Thesis* Grenoble
[5] Nakamura Y 1983 *J. Magn. Magn. Mater.* **31–4** 829
[6] Wada H, Yoshimura K, Shiga M, Goto T and Nakamura Y 1985 *J. Phys. Soc. Japan* **54** 3543
[7] Barret C S and Massalski T B 1986 *Structure of Metals* (New York: McGraw-Hill)
[8] Givord F, Lemaire R and Shah J S 1972 *C. R. Acad. Sci., Paris* B **274** 161
[9] Tagawa Y, Sakurai J, Komura Y, Wada H, Shiga M and Nakamura Y 1985 *J. Phys. Soc. Japan* **54** 591
[10] Ballou R, Lacroix C and Regueiro M D 1991 *Phys. Rev. Lett.* C **66** 1910
[11] Ritter R, Kilcoyne S H and Cywinski R 1991 *J. Phys.: Condens. Matter* **3** 727